Instabilities of nontrivial-phase solutions of the cubic nonlinear Schrödinger equation

Draft - August 22, 2005

Abstract

We consider the two dimensional cubic nonlinear Schrödinger (NLS) equation, which admits a large family of one-dimensional traveling wave solutions. All such bounded solutions may be written in terms of an amplitude and a phase. If the phase of this solution is dependent on the spatial dimension of the one-dimensional wave form, this solution is referred to as having nontrivial phase (NTP). We study the spectral stability analysis of such NTP solutions numerically, using Hill's method. We present evidence which suggests that all such NTP solutions are unstable with respect to transverse perturbations. This transverse instability occurs in both the elliptic and hyperbolic NLS equations, and in the focusing and defocusing case.

1 Introduction

The cubic nonlinear Schrödinger (NLS) equation in two spatial dimensions is given by

$$i\psi_t + \alpha\psi_{xx} + \beta\psi_{yy} + |\psi|^2\psi = 0. \tag{1}$$

The NLS equation is said be *focusing* or *attractive* in the x-dimension if $\alpha > 0$. If $\alpha < 0$, NLS is said to be *defocusing* or *repulsive* in the x-dimension. Similarly, the sign of β will lead to focusing or defocusing in the y-dimension [15]. The NLS equation is called *hyperbolic* if $\alpha\beta < 0$ and *elliptic* if $\alpha\beta > 0$. This equation admits a large family of one-dimensional traveling-wave solutions. A class of these solutions may be written in the form

$$\psi(x,t) = \phi(x)e^{i\theta(x)+i\lambda t}, \tag{2}$$

where $\phi(x)$ and $\theta(x)$ are real-valued functions, and λ is a real constant. Bounded solutions of the form (2) are possible if

$$\phi^2(x) = \alpha\left(-2k^2\,\mathrm{sn}^2(x,k) + B\right), \tag{3a}$$

$$\theta(x) = c\int_0^x \phi^{-2}(\xi)d\xi, \tag{3b}$$

$$\lambda = \frac{1}{2}\alpha(3B - 2(1+k^2)), \tag{3c}$$

$$c^2 = -\frac{\alpha^2}{2}B(B-2k^2)(B-2), \tag{3d}$$

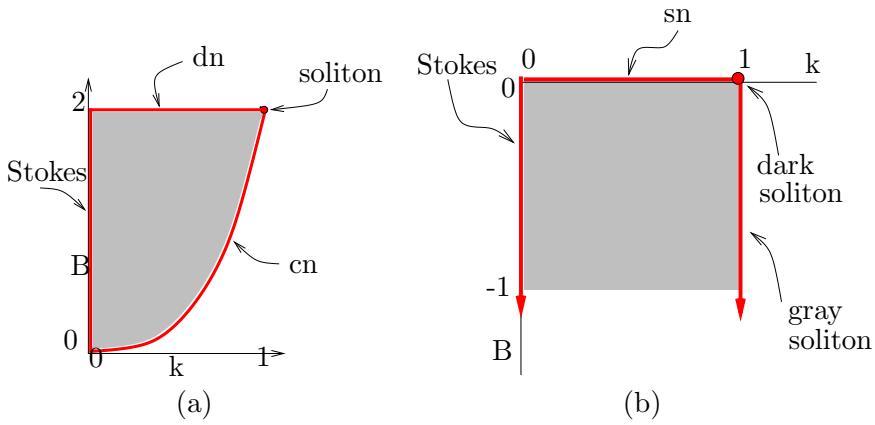

Figure 1: Admissible parameter space for (a) focusing ($\alpha = 1$) and (b) defocusing ($\alpha = -1$) regimes

where c is a real constant. Here $k \in [0, 1]$ is the elliptic modulus of the Jacobi elliptic sine function, $\mathrm{sn}\,(x, k)$. The function $\mathrm{sn}\,(x, k)$ is periodic if $k \in [0, 1)$, with period given by $L = 4K$, with K defined by

$$K(k) = \int_0^{\pi/2} \left(1 - k^2 \sin^2 x\right)^{-1/2} \, dx,$$

the complete elliptic integral of the first kind [2]. When $k = 0$, $\mathrm{sn}\,(x, 0) = \sin(x)$ with $L = 2\pi$. As k approaches 1, $\mathrm{sn}\,(x, k)$ limits to $\tanh(x)$ and L approaches infinity.

The solution ψ is said to have *trivial phase* (TP) if $\theta(x)$ is (piecewise) constant and *nontrivial phase* (NTP) if $\theta(x)$ is not constant. For every choice of α and β, (**??**) specifies a two-parameter family of solutions in the free parameters k and B. Without loss of generality, both α and β are chosen to be ± 1. The phase contribution $\theta(x)$ of (3b) implicitly depends on α and B in both (3a) and (3d). In order for ϕ and θ to be real-valued functions, we need $B \in [2k^2, 2]$ if $\alpha = 1$ or $B \leq 0$ if $\alpha = -1$. Figure 1 represents the (k, B)-parameter space corresponding to nontrivial phase solutions of NLS. As the phase θ approaches zero, the solutions approach one of five simpler types of TP solutions; (*i*) a Stokes wave, (*ii*) a cn-type solution, (*iii*) a dn-type solution, (*iv*) an sn-type solution, (*v*) a soliton-type solutions. Expressions for these simpler solutions are given in Table 1, and the values of k and B which cause (2) to limit to these solutions. Details of the Jacobi elliptic functions sn,cn and dn may be found in [2]. The limiting solutions correspond to the boundaries of the regions in Fig. 1.

While both TP and NTP solutions are of interest, TP results are reasonably well represented in the literature; for example, see [18, 7, 4, 1, 11, 3, 14, 13], although much of this attention has focused on the stability of solitary wave solutions. We know of only Infeld and Ziemkiewicz's paper which considers NTP stability [9]. The linear stability analysis and the large parameter space that needs to be explored makes the NTP setting more complex that the TP setting. The TP solutions will provide a reference for later discussion, when we refer to the stokes, sn, cn and dn type solutions. In this paper, we investigate the spectral stability of all NTP solutions (2), for all possible choices of α and β. That is, we compute the eigenvalues of an approximate spectral problem in order to identify the possible growth instabilities.

TP/NTP solution	ψ	NTP ($\alpha=-1$)	NTP ($\alpha=1$)
Stokes		$k=0, B\leq 0$	$k=0, 0\leq B\leq 2$
cn	$\pm\sqrt{2\alpha}k\,\mathrm{cn}\,(x,k)e^{i\alpha(2k^2-1)t}$	N/A	$0\leq k<1, B=2k^2$
dn	$\pm\sqrt{2\alpha}k\,\mathrm{dn}\,(x,k)e^{i\alpha(2-k^2)t}$	N/A	$0\leq k<1, B=2$
sn	$\pm\sqrt{-2\alpha}k\,\mathrm{sn}\,(x,k)e^{-i\alpha(1+k^2)t}$	$0\leq k<1, B=0$	N/A
Bright soliton	$\pm\sqrt{2\alpha}\mathrm{sech}(x)e^{i\alpha t}$		$k=1, B=2$
Gray soliton	$\pm\sqrt{2\alpha}\tanh(x)e^{2i\alpha t}$	$k=1, B<=0$	

Table 1: I need to work on this table still. TP and NTP solutions coincide for the parameter choices given column 3 and 4 of this table. The name of the solution and its explicit form are given in rows 1 and 2, respectively.

2 The linearized stability problem

In order to study the linear stability of NTP solutions of the NLS equation, we consider perturbations of the form

$$\psi_{_p}(x,y,t)=(\phi(x)+\epsilon u(x,y,t)+i\epsilon v(x,y,t)+\mathcal{O}(\epsilon^2))\mathrm{e}^{i\theta(x)+i\lambda t}, \tag{4}$$

where $u(x,y,t)$ and $v(x,y,t)$ are real-valued functions, ϵ is a small real parameter and $\phi(x)\mathrm{e}^{i\theta(x)+i\lambda t}$ is a NTP solution of NLS. Substituting (4) in (1), linearizing and separating real and imaginary parts leads to

$$\lambda u-3\gamma\phi^2u-\beta u_{yy}+\alpha c^2\frac{1}{\phi^4}u-2\alpha c\frac{1}{\phi^3}\phi_x v+2\alpha c\frac{1}{\phi^2}v_x-\alpha u_{xx}=-v_t, \tag{5a}$$

$$\lambda v-\gamma\phi^2v-\beta v_{yy}+\alpha c^2\frac{1}{\phi^4}v+2\alpha c\frac{1}{\phi^3}\phi_x u-2\alpha c\frac{1}{\phi^2}u_x-\alpha v_{xx}=u_t. \tag{5b}$$

Since (5) does not depend on y or t explicitly, we may assume that $u(x,y,t)$ and $v(x,y,t)$ have the form

$$u(x,y,t)=U(x,\rho,\Omega)\mathrm{e}^{i\rho y+\Omega t}+c.c., \tag{6a}$$

$$v(x,y,t)=V(x,\rho,\Omega)\mathrm{e}^{i\rho y+\Omega t}+c.c., \tag{6b}$$

where ρ is a real constant, $U(x)$ and $V(x)$ are complex-valued functions, Ω is a complex constant and *c.c.* denotes complex conjugate. Notice that ρ is the wave number of the transverse perturbation and Ω is the exponential growth constant associated with ρ. If bounded U,V exist such that Ω has a positive real part, then the amplitudes of the perturbations grow exponentially in time and the unperturbed solution is said to be unstable. Upon substitution, (5) gives

$$\lambda U-3\gamma\phi^2U+\beta\rho^2U+\alpha c^2\frac{1}{\phi^4}U-2\alpha c\frac{1}{\phi^3}\phi_x V+2\alpha c\frac{1}{\phi^2}V_x-\alpha U_{xx}=-\Omega V, \tag{7a}$$

$$\lambda V-\gamma\phi^2V+\beta\rho^2V+\alpha c^2\frac{1}{\phi^4}V+2\alpha c\frac{1}{\phi^3}\phi_x U-2\alpha c\frac{1}{\phi^2}U_x-\alpha V_{xx}=\Omega U. \tag{7b}$$

If $c=0$, then (7) reduces to the stability analysis of trivial phase solutions. This case is examined in [4, 3, 9, 16, 17, 5] and others. With the linear system (7) constructed, we are now able to investigate the stability of the perturbed NTP solution numerically. **SPECTRAL STABILITY**

3 Numerical investigation of spectral stability

The main problem for the numerical investigation of (7) is the size of the parameter space involved. For every choice of the equations parameters α, β and solution parameter pairs (k, B), the spectrum of (7) needs to computed for a range of ρ values to determine stability or to analyze any instabilities. To this end, the efficiency of the numerical method is crucial. The exponential convergence of Hill's method, demonstrated in [6], allows for the systematic exploration of the large phase space encountered here.

3.1 Method

To apply Hill's method, Fourier expansions are needed for all coefficients of (7). Using the complex Fourier form, we have

$$\begin{aligned} \phi^2(x) &= \sum_{k=-\infty}^{\infty} Q_k e^{i2k\pi x/L}, & \phi^{-2}(x) &= \sum_{k=-\infty}^{\infty} R_k e^{i2k\pi x/L}, \\ \phi^{-4}(x) &= \sum_{k=-\infty}^{\infty} S_k e^{i2k\pi x/L}, \quad \text{and} & \phi^{-3}(x)\phi'(x) &= \sum_{k=-\infty}^{\infty} T_k e^{i2k\pi x/L}, \end{aligned} \tag{8}$$

where Q_k, R_k, S_k and T_k are the Fourier coefficients. We note that $\phi^2(x)$ has period $L/2$ and that $\phi(x)$ is never zero except in the TP limit cases.

The periodicity of the coefficients containing powers of ϕ allows us to decompose the eigenfunctions of U and V of the spectral problem in a Fourier-Floquet form

$$U(x) = e^{i\mu x} \sum_{l=-\infty}^{\infty} U_l e^{-il\pi x/L} \quad \text{and} \quad V(x) = e^{i\mu x} \sum_{l=-\infty}^{\infty} V_l e^{-il\pi x/L}. \tag{9}$$

The form of U and V in (9) follows from Floquet's theorem and the observation that we seek eigenfunctions, which are by definition bounded. This decomposition has the benefit of admitting both periodic and anti-periodic eigenfunctions. Allowing the Floquet multiplier μ to be different from 0 admits solutions with periodicity other than L. Again, see [6] for a more complete explanation and discussion.

Substitution of (8) and (9) in (7) allows us to write equations for U_n and V_n as a coupled bi-infinite system of difference equations given by

$$\begin{aligned} -\left(\lambda + \beta\rho^2 - \alpha\left(i\mu + \frac{in\pi}{L}\right)^2\right) U_n + 3\gamma \sum_{k=-\infty}^{\infty} Q_{\frac{n-k}{2}} U_k - \alpha c^2 \sum_{k=-\infty}^{\infty} S_{\frac{n-k}{2}} U_k \\ + 2\alpha c \sum_{k=-\infty}^{\infty} T_{\frac{n-k}{2}} V_k - 2\alpha c\left(i\mu + \frac{in\pi}{L}\right) \sum_{k=-\infty}^{\infty} R_{\frac{n-k}{2}} V_k = \Omega V_n \end{aligned} \tag{10a}$$

$$\begin{aligned} \left(\lambda + \beta\rho^2 - \alpha\left(i\mu + \frac{in\pi}{L}\right)^2\right) V_n - \gamma \sum_{k=-\infty}^{\infty} Q_{\frac{n-k}{2}} V_k + \alpha c^2 \sum_{k=-\infty}^{\infty} S_{\frac{n-k}{2}} V_k \\ + 2\alpha c \sum_{k=-\infty}^{\infty} T_{\frac{n-k}{2}} U_k - 2\alpha c\left(i\mu + \frac{in\pi}{L}\right) \sum_{k=-\infty}^{\infty} R_{\frac{n-k}{2}} U_k = \Omega U_n, \end{aligned} \tag{10b}$$

Parameter	Description	value
k	Elliptic Modulus	`linspace(0,1,65)`
B	Shift	For $\alpha = -1$: $-$`logspace(`$-8, 0, 65$`)` For $\alpha = \ \ 1$: $(2k^2 +$ `logspace(`$-8, 0, 65$`)`$) \cap (2k^2, 2)$
N	Fourier cutoff	For $\alpha = -1 : 15 +$ `ceil(`$5\mathtt{k}^5$`)` For $\alpha = \ \ 1 : 10 +$ `ceil(`$25\mathtt{k}^{10}$`)`
ρ	perturbation wavenumber	`linspace(0,4,65)`
μ	Floquet parameter	`linspace(`$-\frac{\pi}{\mathtt{K}}, \frac{\pi}{\mathtt{K}}, 21$`)`

Table 2: Parameter values and ranges used in numerical experiments.

which hold for all integers n. Here $\mu \in [\frac{-\pi}{K}, \frac{\pi}{K})$ and $Q_{\frac{n-k}{2}} = 0$ if $n - k \notin 2\mathbb{Z}$, with $R_{(\cdot)}, S_{(\cdot)}$ and $T_{(\cdot)}$ similarly defined. Equations (10a) and (10b) are *equivalent* to the original system (7).

In practice, a pre-multiplication of the linear system by ϕ^4 allows for an exact cosine series expansion of ϕ^2, ϕ^4 and ϕ^6 to be used. This follows from the differential equations for $\mathrm{sn}\,(x,k)$ and Jacobi's [10] series expansion of $\mathrm{sn}^{\,2}(x,k)$. This pre-multiplication transforms the original eigenvalue problem into a generalized eigenvalue problem. Golub and Van Loan [8] provide a brief discussion of generalized eigenvalue problems. For details of the numerical technique, see [12].

3.2 Numerical Experiments

Equations (10a) and (10b) are the foundation for the numerical experiments. By first choosing a finite number of Fournier modes, and then truncating the exact bi-infinite system (10) at this point, we can explicitly construct and compute the eigenvalues of a finite dimensional matrix approximation. We consider all four cases: (I) focusing in x and focusing in y ($\alpha = \beta = 1$), (II) focusing in x and defocusing in y ($\alpha = -\beta = 1$), (III) defocusing in x and focusing in y ($-\alpha = \beta = 1$) and finally, (IV) defocusing in x and defocusing in y ($-\alpha = -\beta = 1$).

In each case, a large number of parameter values in the two dimensional parameter space shown in Fig. 1 was explored numerically. Approximately 5.2 million generalized eigenvalue problems were considered, the size of each determined by the cutoff mode N of the underlying Fourier series. A truncation to N positive Fourier coefficients reduces the bi-infinite exact system (10) to an approximate $(4N + 2)$-dimensional problem. For several random values of k and B, the value $N(k, B)$ was chosen to ensure that the resulting eigenvalues had converged to within a measured tolerance. A simple polynomial was used to fit this data. This information, and details related to other parameter ranges used in the experiments, are included in Table 2. In the table, k is the elliptic modulus, B may be interpreted as a measure of the nontrivial phase quantity θ, $(4N + 2)$ is the matrix dimension used to approximate the full operator, ρ is the wave number of the perturbation in the y-dimension, and μ is the Floquet parameter. Also, `linspace(a,b,m)` is a linearly spaced vector from a to b of length m, `logspace(a,b,m)` is a logarithmically spaced vector from 10^a to 10^b of length m and function `ceil(x)` is the smallest integer not less than x.

3.3 Results

First and foremost, it should be stated that *none* of the solutions considered here were found to be spectrally stable. This establishes, at least numerically, that *all* one-dimensional traveling-wave

solutions of NLS are unstable. At this point, it remains to investigate the nature of the instabilities, so as to better understand the dynamics of this important class of solutions of the NLS equation.

Using the Hill method we numerically considered the instabilities due to transverse perturbations with wavenumber denoted by $\rho \in [0, 4]$. For each NLS equation (*i.e.* for each choice of $\alpha, \beta = \pm 1$), and for each parameter pair (k, B), and for each perturbation of wave number ρ, a sequence of a sequence of Floquet parameters μ was chosen from the interval $[\frac{-\pi}{K}, \frac{\pi}{K}]$. The generalized eigenvalues and eigenvectors were computed from the resulting matrix. The eigenvalues are approximations of spectral elements of (7), and an approximation of the corresponding eigenfunctions may be reconstituted from the generalized eigenvectors.

Since a single eigenvalue with positive real part will lead to instability of the system, the eigenvalue with largest real part over all choices of μ was recorded for each (k, B, ρ) triplet. That is, we compute

$$\Omega_{growth}(k, B, \rho) = \max_{\mu \in [-\pi/2L, \pi/2L]} Re\Omega(k, B, \rho, \mu),$$

which we call the growth rate for a given NTP solution with solution parameters k, B and perturbed with transverse wavenumber ρ. We reduce the dimension still further by computing the largest such growth rate over all sampled perturbation wavenumbers ρ. This quantity,

$$\Omega_{\max}(k, B) = \max_{\rho \in [0,4]} \Omega_{growth}(k, B, \rho),$$

the maximal growth rate over all ρ, is plotted in the first column of Figs. 2 and 3. This represents the maximal exponential growth rate a solution with parameters (k, B) can undergo, and allows us to determine the solution which is spectrally the most unstable. We also recorded the minimum growth rate over all ρ,

$$\Omega_{\min}(k, B) = \min_{\rho \in [0,4]} \Omega_{growth}(k, B, \rho),$$

to verify that all solutions are unstable with respect to at least one transverse perturbation.

The plots in Fig. 2 correspond the x-focusing parameter range $(k, B) = (0, 1) \times (2k^2, 2)$ in the $\alpha = 1$ case of Fig. 1(a). The one-to-one transform $T_f(B) = (B - 2k^2)/(2 - 2k^2)$ is used to normalize the range of B. This maps the interval $[2k^2, 2]$ to $[0, 1]$. The plots in 3 correspond to the x-defocusing parameter range of $(k, B) = (0, 1) \times (-1, 0)$ shown in Fig. 1(b). The transform $T_d(B) = -B$ is used in III and IV. Every point in the plots of Figs. 2 and 3 corresponds to a solution, and the boundaries in the figure are the boundaries of the regions represented in Fig. 1 and correspond to the limiting TP solutions. The column on the right of Figs. 2 and 3 indicates the wavenumber ρ which leads to maximal growth. Recall that our computations were truncated at $\rho = 4$, and so in all cases the maximum or minimum may occur at values of $\rho > 4$. An observed value of $\rho = 4$ indicates that there is a strong short-wavelength (large ρ) instability.

3.3.1 Case I: $\alpha = \beta = 1$

The plots Ia and Ib of Fig. 2 summarize the computed instabilities in the case of focusing in both the x- and y -dimensions. This setting is applicable to nearly monochromatic waves of small amplitude in pulse propagation in optical waves. This is the setting which limits to the bright solitons for $k = 1$. Recall that the original parameter space corresponds to $(k, B) = (0, 1) \times (2K^2, 2)$, and that the map T_f is used to transform this to $(0, 1) \times (0, 1)$. This transform, coupled with the $\log_{10}$ scaling, causes the plots to become increasingly sparse towards the right bottom corner. The

lower boundary of the plot corresponds to $B = 2k^2 + (10^{-8})$, and so is just slightly away (in the parameter space of B) from a cn-type solution. The upper boundary is close to dn-type solution, with $B = 1.99$. The left boundary of the plots, where $k = 0.01$, represents a region in parameter space near to Stokes wave solutions, while $k = 0.99$ on the left boundary. The limit case where $(k, B) = (1, 2)$ corresponds to the bright soliton.

A distinct ridge of large instability is noticeable in the growth plot I(a). The ridge appears to begin near the trivial limit $k = 0$ and $B = 0$, and remains close to the cn limit boundary (within approximately .02 units) as k increases, and reaches a global maximum of $R_{\max} = 5.666$ near $k = 0.96$. The growth plot I(a) also indicates that system stability factor grows quickly for fixed k as B moves away from the cn TP solution at the bottom the plot. After this point, increasing B causes the growth factor to decrease, although this time more slowly, as the dn TP solution is approached at the top edge of the plot. This suggests that for fixed k, the cn-type solution loses stability much more quickly (in B parameter space) than does a corresponding dn-type solution. For fixed B, the stability increases slowly as k varies from 0 to 1.

In Ib, the wavelength corresponding to the maximal growth of I(a) are given. In this case, the maximum instability occurs for the shortest wavelength samples, $\rho = 4$. This indicates that there is a strong short-wavelength (large ρ) instability, although a larger growth rate might be observed for a larger value of ρ.

3.3.2 Case II: $\alpha = -\beta = 1$

Plots IIa and IIb of Fig. 2 summarize the computed instabilities in the case of focusing in the x-dimension and defocusing in the y-dimension. This case applies to deep water waves rather then optical wave pulses. The lower boundary of the plot corresponds to $B = 2k^2 + (10^{-8})$, and so is just slightly away (in parameter space of B) from a cn-type solution. The upper boundary is close to dn-type solution, with $B = 1.99$. The left boundary of the plots, where $k = 0.01$, represents a region in parameter space near to Stokes wave solutions, while $k = 0.99$ on the left boundary. The bright soliton solution is the limiting case result when $k \to 1$.

As in Case I, a ridge of large instability is noticeable in the growth plot IIa. The ridge appears to begin near the trivial limit $k = 0$ and $B = 0$, and remains close to the cn limit boundary (within approximately .02 units) as k increases, then decreases to reach a local minimum near $k = 0.7$ and increases again to a global minimum near $k = 0.96$. Plot II(a) indicates that system stability factor grows quickly for fixed k as B moves away from the cn TP solution at the bottom the plot. After this point, increasing B causes the growth factor to decrease, although this time more slowly, as the dn TP solution is approached at the top edge of the plot. This suggests that for fixed k, the cn-type solution loses stability much more quickly (in this parameter space) than does a corresponding dn-type solution. In comparison to this rapid loss of stability for fixed k, the stability increases more slowly for fixed B as k varies from 0 to 1. The maximum ($R_{\max} = 6.1141$) and minimum ($R_{\min} = 0.012535$) growth rates span a slightly larger range than the similar values in Fig. 2.

In IIb, the wavelength corresponding to the maximal growth of IIa are given. In this case, the maximum instability of R_{max} occurs for $\rho = 3.375$. The surface represented by IIb appears to be much smoother than the surface of Ib.

3.3.3 Case III: $-\alpha = \beta = 1$

Plots IIIa and IIIb of Fig. 3 summarize the computed instabilities in the case of defocusing in the x-dimension and focusing y-dimension. These plots again correspond to the deep water setting. The lower limit of the plot corresponds to $B = -(10^{-8})$, and so is just slightly away from the sn solution. The left boundary of the plots, where $k = 0.01$, represents a region in parameter space near to Stokes wave solutions, while $k = 0.99$ on the left boundary. In the limit as $k \to 1$, the solution becomes a gray soliton.

A distinct ridge of large instability is noticeable in the growth plot III(a). The ridge appears to begin near the trivial limit $k = 0$ and $B = 0$, and remains close to the sn limit boundary (within approximately .02 units) as k increases, to reach a global maximum near $k = 0.02$ and $B = -0.0001$. The ridge then appears to decrease in amplitude as k increases towards 1. For solutions near the Stokes wave limit, $k = 0$, the solutions appear to lose stability quickly as k increases, but that an increase in B will delay this process. The increase in the growth rate is most rapid near the sn-type solution limit at $B = 0$. The maximum exponential growth rate occurs for a small k near the Stokes wave boundary of $k = 0$. and is given by $R_{max} = 7.6375$ and minimum $R_{\min} = .015578$.

The plot IIIa indicates that much of large growth in this setting is attributable to short wave perturbations. The largest growth occurs for a perturbation with wavenumber of $\rho = 3.625$.

3.3.4 Case IV: $-\alpha = -\beta = 1$

The plots IVa and IVb of Fig. 3 summarize the computed instabilities in the case of defocusing in both the x- and y-dimensions. As in Case I, this setting is applicable to nearly monochromatic waves of small amplitude in pulse propagation in optical fiber. The lower limit of the plot corresponds to $B = -(10^{-8})$, and so is just slightly away from the sn solution, as measured in the parameter B. The left boundary of the plots, where $k = 0.01$, represents a region in parameter space near to the Stokes wave solutions, while $k = 0.99$ on the left boundary. In the limit as $k \to 1$, the solutions become grey solitons.

A distinct ridge of large instability is noticeable in the growth plot IVa. The ridge appears to begin near the trivial limit $k = 0$ and $B = 0$, and remains close to the sn limit boundary (within approximately .02 units) as k increases, to reach a global maximum near $k = 0.02$ and $B = -0.0001$. The ridge then appears to decrease in amplitude as k increases towards 1. For solutions near the Stokes wave limit, $k = 0$, the solutions appear to lose stability quickly as k increases. An increase of B will delay this process. The increase in the growth rate is most rapid near the sn-type solution limit at $B = 0$, and the maximal growth rate $R_{\max} = 7.6456$ and the minimum growth rate of $R_{\min} = 0.0001556$.

In IVb the wavenumbers corresponding to the maximal growth of IVa are plotted. It appears that a majority of the maximal instability is attributable to small ρ (long wave) perturbations. In fact, the largest growth occurs for $\rho = 0$, the one-dimensional perturbation. This is different than in the previous plots I-IIIb, where short wave perturbations were associated with much of the large growth rate.

4 Summary

In this paper, we have considered the spectral instability of one-dimensional traveling wave NTP solutions of the cubic nonlinear Schrödinger equation. The solutions used are formulated in terms

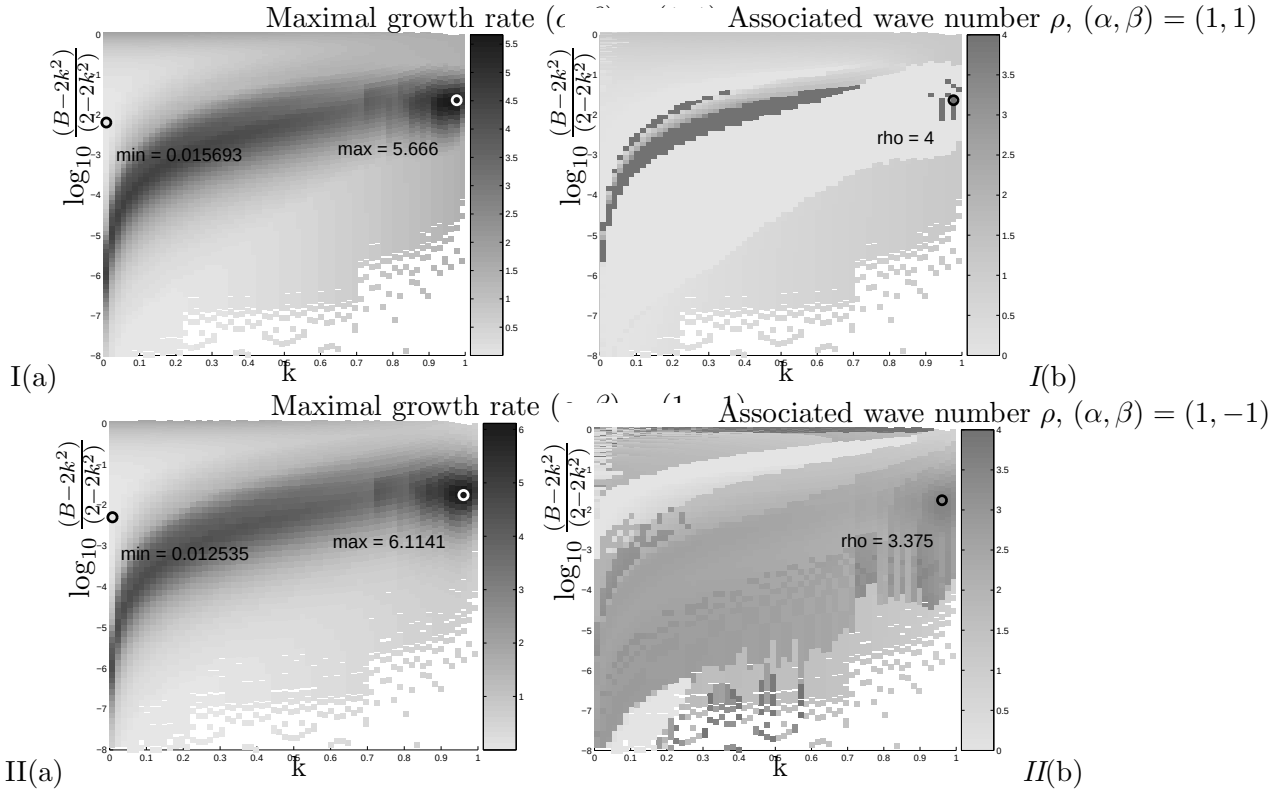

Figure 2: Plots representing (a) maximum spectral growth for $\rho \in [0, 4]$ and (b) indicating corresponding wavenumber leading to instability. Here $R_{\max} = \max_{k,B,\rho} \max_{\mu} Re(\Omega)$ and $R_{\min} = \min_{k,B,\rho} \max_{\mu} Re(\Omega)$. The vertical dimension, measured on a $\log_{10}(B - 2k^2)/(2 - 2k^2)$ scale, indicates the amount of nontrival phase in the underlying solution.

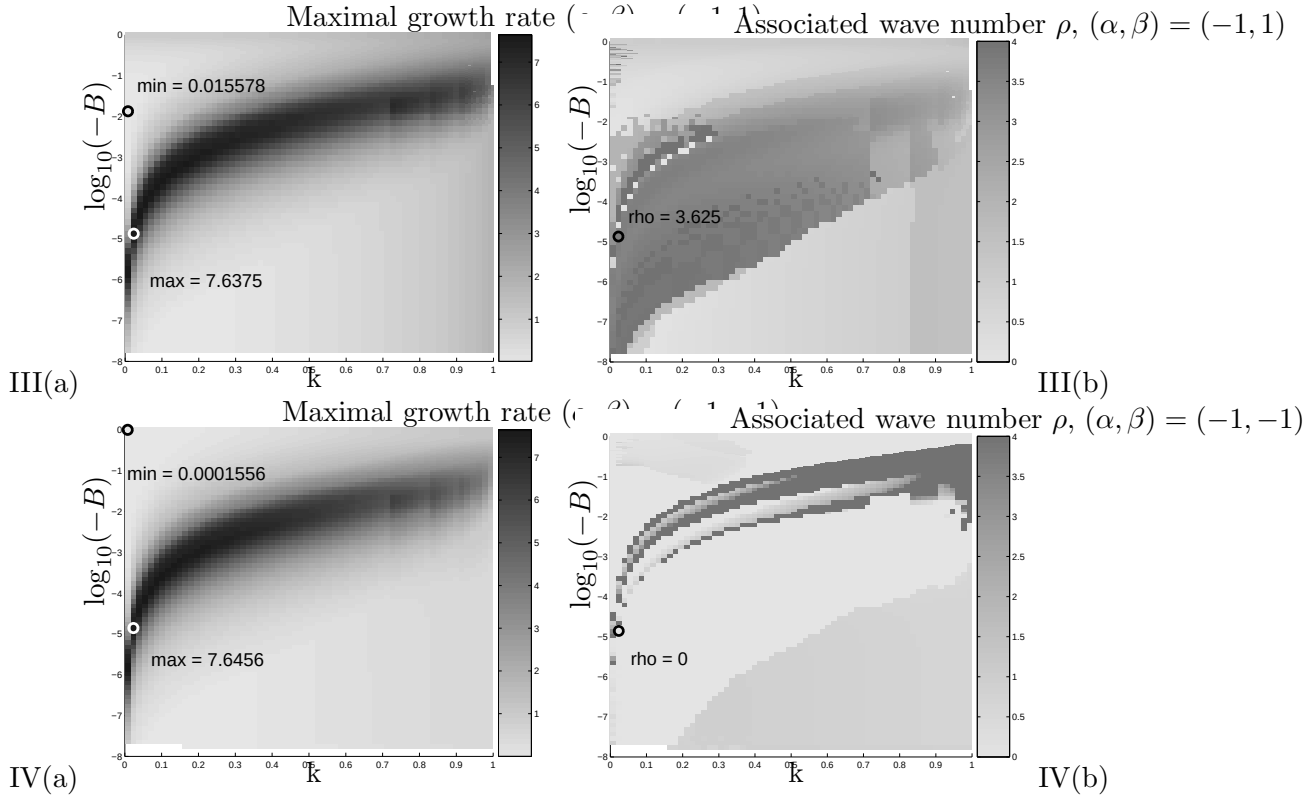

Figure 3: Defocusing x-dimension plots representing (a) maximum spectral growth for $\rho \in [0, 4]$ and (b) indicating corresponding wavenumber leading to instability. Here $R_{\max} = \max_{k,B,\rho}(\max_{\mu}(Re(\Omega)))$ and $R_{\min} = \min_{k,B,\rho}(\max_{\mu}(Re(\Omega)))$. The vertical dimension, measured on the $\log_{10}(-B)$ scale, indicates the amount of nontrivial phase in the underlying solution.

of Jacobi elliptic functions. An exact spectral form of the linearized operator is discretized and used to construct an associated generalized eigenvalue problem. The positive real part of the resulting eigenvalues was used to determine that *none* of the solutions considered are spectrally stable. The numerics indicate a well-defined ridge of maximal instability which is located in the (k, B)-parameter region associated with fully nontrivial phase solutions. In addition, the numerical evidence indicates that exponential growth rates of dn-type solutions, and to a lesser extent the Stokes wave solutions, are robust under transverse perturbation. The growth of the cn-type and sn-type solutions appear to be quite sensitive to this perturbation. In summary, numerical evidence suggests that bounded, nontrivial one dimensional traveling wave solutions to the cubic NLS equation are unstable under transverse perturbation, and we have characterized the nature of this instability.

References

[1] V. A. Aleshkevich, A. A. Egorov, Y. V. Kartashov, V. A. Vysloukh, and A. S. Zelenina. Stability of spatiotemporal cnoidal waves in cubic nonlinear media. *Phys. Rev. E*, 67:066605, 2003.

[2] P. F. Byrd and M. D. Friedman. *Handbook of Elliptic Integrals for Engineers and Physicists.* Springer-Verlag, 1954.

[3] J. Carter and B. Deconinck. Stability of trivial phase solutions of the two-dimensional cubic nonlinear Schrödinger equation. *submitted for publication*, 2005.

[4] J. Carter and H. Segur. Instability in the two-dimensional cubic nonlinear Schrödinger equation. *Phys. Rev. E.*, 68(4):045601, 2003.

[5] B. Deconinck and J. N. Kutz. Computing spectra of linear operators using Hill's method. *submitted for publication*, 2005.

[6] B. Deconinck, D. E. Pelinovsky, and J.D. Carter. Transverse instabilities of deep-water solitary waves. *submitted for publication*, 2005.

[7] S. E. Fil'chenkov, G. M. Fraiman, and A. D. Yunakovskii. Instability of periodic solutions of the nonlinear Schrödinger equation. *Sov. J. Plasma Phys.*, 18(8):961–966, 1987.

[8] G. H. Golub and C. F. Van Loan. *Matrix Computations.* Johns Hopkins University Press, 1996.

[9] E. Infeld and J. Ziemkiewicz. Stability of complex solutions of the nonlinear Schrödinger equation. *Acta Phys. Pol.*, A59(3):255, 1981.

[10] C.G. Jacobi. *Fundamenta Nova Theoriae Functionum Ellipticarum.* Königsberg, 1829.

[11] Y. V. Kartashov, V.A. Aleshkevich, V.A. Vysloukh, A.A. Egorov, and A.S. Zelenina. Transverse modulational instability of (2+1)-dimensional cnoidal waves in media with cubic nonlinearity. *J. Opt. Soc. Am. B.*, 20(6):1273–1284, 2003.

[12] Y. S. Kivshar and D. E. Pelinovsky. Self-focusing and transverse instabilities of solitary waves. *Phys. Rep.*, 331(4):118–195, 2000.

[13] E.A. Kuznetsov, A.M. Rubenchik, and V.E. Zakharov. Soliton stability in plasmas and hydrodynamics. *Phys. Rep.*, 142:103–165, 1986.

[14] D. U. Martin, H. C. Yuen, and P. G. Saffman. Stability of plane wave solutions of the two-space-dimensional nonlinear Schrödinger equation. *Wave Motion*, 2:215–229, 1980.

[15] C.B. Moler and G.W. Stewart. An algorithm for generalized matrix eigenvalue problem. *SIAM J. Numer. Anal.*, 10(2), 1973.

[16] K. Rypdal and J. J. Rasmussen. Stability of solitary structures in the nonlinear Schrödinger equation. *Physica Scripta*, 40:192, 1989.

[17] P. L. Sulem and C. Sulem. *Nonlinear Schrödinger Equations: Self-focusing and Wave Collapse.* Springer-Verlag, NY, 1999.

[18] V. E. Zakharov and A. M. Rubenchik. Instability of waveguides and soliton in nonlinear media. *Sov. Phys. JETP*, 38(3):494–500, 1974.